2

Bandpass Sampling for Data Acquisition Systems

Leopoldo Angrisani[1] and Michele Vadursi[2]
[1]*University of Naples Federico II, Department of Computer Science and Control Systems*
[2]*University of Naples "Parthenope", Department of Technologies*
Italy

1. Introduction

A number of modern measurement instruments employed in different application fields consist of an analogue front-end, a data acquisition section, and a processing section. A key role is played by the data acquisition section, which is mandated to the digitization of the input signal, according to a specific sample rate (Corcoran, 1999).
The choice of the sample rate is connected to the optimal use of the resources of the data acquisition system (DAS). This is particularly true for modern communication systems, which operate at very high frequencies. The higher the sample rate, in fact, the shorter the observation interval and, consequently, the worse the frequency resolution allowed by the DAS memory buffer. So, the sample rate has to be chosen high enough to avoid aliasing, but at the same time, an unnecessarily high sample rate does not allow for an optimal exploitation of the DAS resources.
As well known, the sample rate must be correctly chosen to avoid aliasing, which can seriously affect the accuracy of measurement results. The sampling theorem, in fact, affirms that a band-limited signal can be alias-free sampled at a rate f_s greater than twice its highest frequency f_{max} (Shannon, 1949).
As regards bandpass signals, which are characterized by a low ratio of bandwidth to carrier frequency and are peculiar to many digital communication systems, a much less strict condition applies. In particular, bandpass signals can be alias-free sampled at a rate f_s greater than twice their bandwidth B (Kohlenberg, 1953). It is worth noting, however, that this is only a necessary condition. It is indeed possible to alias-free sample bandpass signals at a rate fs much lower than $2f_{max,}$ but such rate has to be chosen very carefully; it has been shown in (Brown, 1980; Vaughan et al., 1991; De Paula & Pieper, 1992; Tseng, 2002) that aliasing can occur if fs is chosen outside certain ranges. Moreover, particular attention has to be paid, as bandpass sampling can imply a degradation of the signal-to-noise ratio (Vaughan et al., 1991). Some recent papers have also focused on frequency shifting induced by bandpass sampling in more detail (Angrisani et al. 2004; Diez et al., 2005), providing analytical relations for establishing the final central frequency of the discrete-time signal, which digital receivers need to know (Akos et al., 1999) and determining the minimum admissible value of fs that is submultiple of a fixed sample rate (Betta et al., 2009).
Sampling a bandpass signal at a rate lower than twice its highest frequency f_{max} is referred to as bandpass sampling. Bandpass sampling is relevant in several fields of application, such

as optics (Gaskell, 1978), communications (Waters & Jarrett, 1982), radar (Jackson & Matthewson, 1986) and sonar investigations (Grace & Pitt, 1968). It is also the core of the receiver of software-defined radio (SDR) systems (Akos et al., 1999; Latiri et al., 2006).
Although the theory of bandpass sampling is now well-established and the choice of sample rate is very important for processing and measurement, at the current state of the art it seems that digital instruments that automatically select the best f_s, on the basis of specific optimization strategies, are not available on the market. A possible criterion for choosing the optimal value of f_s within the admissible alias-free ranges was introduced some years ago (Angrisani et al., 2004). An iterative algorithm was proposed, which selects the minimum alias-free sample rate that places the spectral replica at the normalized frequency requested by the user. The algorithm, however, cannot be profitably applied to any DAS. Two conditions have, in fact, to be met: (*i*) the sample rate can be set with unlimited resolution, and (*ii*) the sample clock has to be very stable. Failing to comply with such ideal conditions may result in an undesired and unpredictable frequency shifting and possible aliasing.
More recently, a comprehensive analysis of the effects that the sample clock instability and the time-base finite resolution have on the optimal sample rate and, consequently, on the central frequency of the spectral replicas was developed (Angrisani & Vadursi, 2008). On the basis of its outcomes, the authors also presented an automatic method for selecting the optimal value of f_s, according to the aforementioned criterion.
The method includes both sample clock accuracy and time-base resolution among input parameters, and is suitable for practical applications on any DAS, no matter its sample clock characteristics. Specifically, the method provides the minimum f_s that locates the spectrum of the discrete-time signal at the normalized central frequency required by the user, given the signal bandwidth B, a possible guard band B_g, and original carrier frequency f_c. Information on the possible deviation from expected central frequency, as an effect of DAS non-idealities, is also made available. In fact, the proposed method is extremely practical, since (i) it can be profitably applied no matter what the time-base resolution of the DAS is, and (ii) it takes into account the instability of the sample clock to face unpredictable frequency shifting and the consequent possible uncontrolled aliasing.
A number of tests are carried out to assess the performance of the method in correctly locating the spectral replica at the desired central frequency, while granting no superposition of the replicas. Some tests are, in particular, mandated to highlight the effects of DAS non-idealities on the frequency shifting and consequent unexpected aliasing.
This chapter is organized as follows. The theory of bandpass sampling will be presented in Section 2, along with analytical relations for establishing the final central frequency of the discrete-time signal and details and explicative figures on the frequency shifting resulting from the bandpass sampling and on the effects of the sample rate choice in terms of possible aliasing. Section 2 also presents the analysis of the effects that the sample clock instability and the time-base finite resolution which was first introduced in (Angrisani & Vadursi, 2008). Section 3 presents the proposed algorithm for the automatic selection of the sample rate given the user's input, and shows the results of experiments conducted on real signals.

2. Analysis of the effects of bandpass sampling with a non-ideal data acquisition system

Let $s(t)$ be a generic bandpass signal, characterized by a bandwidth B and a central frequency f_c. As well known, the spectrum of the discrete-time version of $s(t)$ consists of an infinite set of replicas of the spectrum of $s(t)$, centered at frequencies

$$f_{\lambda,\nu} = \lambda f_c + \nu f_s \tag{1}$$

where $\nu \in \mathbf{Z}$ and $\lambda \in \{-1;1\}$.
The situation is depicted in Fig.1 with regard to positive frequencies of magnitude spectrum.

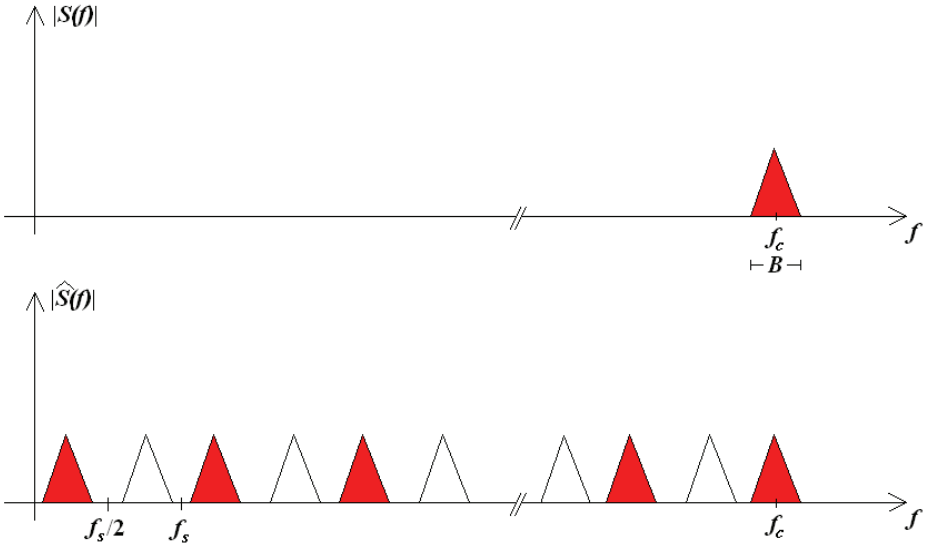

Fig. 1. Typical amplitude spectrum of (a) a bandpass signal s(*t*) and (b) its sampled version; f_s is the sample rate. Only the positive portion of the frequency axis is considered.

Replicas of the 'positive' spectrum (red triangles in Fig.1) are centered at $f_{1,\nu}$, whereas those peculiar to the 'negative' one (white triangles in Fig.1) are centered at $f_{-1,\nu}$. It can be shown that only two replicas are centered in the interval $[0, f_s]$, respectively at frequencies

$$f_{\lambda 1,\nu 1} = f_c \bmod f_s \tag{2}$$

and

$$f_{\lambda 2,\nu 2} = f_s - (f_c \bmod f_s) \tag{3}$$

where mod denotes the modulo operation. The condition to be met in order to avoid aliasing is

$$\frac{B + B_g}{2} < f^* < \frac{f_s - (B + B_g)}{2} \tag{4}$$

where f^* is the minimum $f_{\lambda 1,\nu 1}$ and $f_{\lambda 2,\nu 2}$. Inequality (4) implies the following condition on $(f_c \bmod f_s)$:

$$f_c \bmod f_s \in \left(\frac{B + B_g}{2}, \frac{f_s - (B + B_g)}{2} \right) \cup \left(\frac{f_s + B + B_g}{2}, f_s - \frac{B}{2} \right) \tag{5}$$

The algorithm proposed in (Angrisani et al., 2004) allows the choice of the normalized frequency f^*/f_s , granting a minimum guard band between adjacent replicas, and gives in output the ideal sample rate f_s. However, the problem is not solved yet. In fact, the operative condition provided in (Angrisani et al., 2004) has to cope with the characteristics of an actual DAS. First of all, the sample rate cannot be imposed with arbitrary resolution, but it has to be approximated according to the resolution of the time-base of the DAS. Moreover, the time-base instability makes actual sample rate unpredictable. By the light of this, the actual value of the sample rate given by the DAS could be different from the ideal one in such a way that alias-free sampling could not be guaranteed anymore.
Given the nature of bandpass sampling, simply increasing f_s is not advisable (Vaughan et al., 1991), but an appropriate model is rather needed. Taking into account that: (i) the nominal sample rate, f_s^{nom}, that the user can set on the DAS, differs from f_s of a deterministic quantity ε and (ii) the actual sample rate, f_s' , i.e. the rate at which the DAS actually samples the input signal, is random due to the time-base instability, the following model results:

$$f_s' = f_s^{nom}(1+\chi) = (f_s+\varepsilon)(1+\chi) \tag{6}$$

with

$$|\chi| < \chi_M \tag{6a}$$

$$\varepsilon < \Delta f/2 \tag{6b}$$

where Δf is the resolution and χ_M is the clock accuracy expressed in relative terms, as commonly given in the specifications of the DAS on the market. The actual sample rate f_s' thus differs from the expected value by the quantity

$$\Delta f_s = \chi f_s + (1+\chi)\varepsilon \tag{7}$$

which depends on the output value of the algorithm, f_s.
As alias-free sampling is a strict priority, the model will be specialized in the following letting χ coincide with its maximum value χ_M. Let us separately analyze the two cases $f^* = f_{\lambda 1,\nu 1}$, with a replica of the positive spectrum centered in f^*, and $f^* = f_{\lambda 2,\nu 2}$, with a replica of the negative spectrum centered in f^*.

2.1 Replica of the positive spectrum in (0, f_s/2)

This happens when λ = 1 and $\nu = -\lfloor f_c/f_s \rfloor$, that is the integer part of f_c/f_s. According to (6), the actual value of f^* is

$$f^{*\prime} = f_c + \nu f'_s = f_c + \nu (f_s + \varepsilon)(1+\chi) \tag{8}$$

and (4), evaluated for the actual values of f_s and f^*, yields

$$\frac{B+B_g}{2} + g_1(\varepsilon,\chi) < f^* < \frac{f_s - B + B_g}{2} + g_2(\varepsilon,\chi) \tag{9}$$

where

$$g_1(\varepsilon,\chi) = -\nu\left[\chi f_s + \varepsilon(1+\chi)\right] \tag{10}$$

$$g_2(\varepsilon,\chi)=\left(\frac{1}{2}-\nu\right)\left[\chi f_s+\varepsilon(1+\chi)\right]. \tag{11}$$

To find the pair $\{\varepsilon, \chi\}$ that maximizes $g_1(\varepsilon, \chi)$ in the domain $\mathcal{D} = [-\Delta f/2, \Delta f/2] \times [\chi_M, \chi_M]$ let us first null the partial derivatives of g_1 with respect to variables ε and χ:

$$\begin{cases}-\nu(1+\chi)=0\\ -\nu(f_s+\varepsilon)=0\end{cases}. \tag{12}$$

The system (12) has no solutions in actual situations. Similarly, it can be shown that the restriction of the function to the borders does not have local maxima. The maximum has therefore to be searched among the vertices of the rectangle representing the domain. Table 1 enlists the coordinates of the vertices along with the related values assumed by the function.

As $\nu < 0$, g_1 assumes its maximum in the point C, and the left side of (9) is maximized by

Vertex	*Coordinates*	*Value of g_1*
A	$\left(-\frac{\Delta f}{2},-\chi_M\right)$	$-\nu\left[-\chi_M f_s-\frac{\Delta f}{2}(1-\chi_M)\right]$
B	$\left(-\frac{\Delta f}{2},\chi_M\right)$	$-\nu\left[\chi_M f_s-\frac{\Delta f}{2}(1+\chi_M)\right]$
C	$\left(\frac{\Delta f}{2},\chi_M\right)$	$-\nu\left[\chi_M f_s+\frac{\Delta f}{2}(1+\chi_M)\right]$
D	$\left(\frac{\Delta f}{2},-\chi_M\right)$	$-\nu\left[-\chi_M f_s+\frac{\Delta f}{2}(1-\chi_M)\right]$

Table 1. Values assumed by $g_1(\varepsilon, \chi)$ in the vertices of its domain $\mathcal{D}$.

$$\frac{B+B_g}{2}-\nu\left[\chi_M f_s+\frac{\Delta f}{2}(1+\chi_M)\right]. \tag{13}$$

With regard to the right side of (9), it can be similarly shown that $g_2(\varepsilon, \chi)$ assumes its minimum on one of the vertices of the domain $\mathcal{D}$. The four alternatives are enlisted in Table 2. Being $\nu < 0$, the vertex C can be discarded, because g_2(C) is sum of all positive terms. Moreover, as $\chi_M (f_s - \Delta f/2) > 0$, g_2(A) < g_2(B). Finally, posing g_2(A) < g_2(D) implies $-\Delta f (1 - \chi_M) < 0$, which is always true in actual situations.

In conclusion, g_2 assumes its minimum in A, and the right side of (9) is minimized by

$$\frac{\left(f_s-\frac{\Delta f}{2}\right)(1-\chi_M)-\left(B+B_g\right)}{2}+\nu\left[\chi_M f_s+\frac{\Delta f(1-\chi_M)}{2}\right]. \tag{14}$$

According to (13) and (14), in the most restrictive case the condition (9) can be rewritten as

$$\begin{cases} f^* < \dfrac{\left(f_s - \dfrac{\Delta f}{2}\right)\left(1-\chi_M\right) - \left(B + B_g\right)}{2} + \nu\left[\chi_M f_s + \dfrac{\Delta f\left(1-\chi_M\right)}{2}\right] \\ f^* > \dfrac{B + B_g}{2} - \nu\left[\chi_M f_s + \dfrac{\Delta f}{2}\left(1+\chi_M\right)\right] \end{cases} . \tag{15}$$

Vertex	*Coordinates*	*Value of g_1*
A	$\left(-\frac{\Delta f}{2}, -\chi_M\right)$	$\left(\frac{1}{2}-\nu\right)\left[-\chi_M f_s - \frac{\Delta f}{2}\left(1-\chi_M\right)\right]$
B	$\left(-\frac{\Delta f}{2}, \chi_M\right)$	$\left(\frac{1}{2}-\nu\right)\left[\chi_M f_s - \frac{\Delta f}{2}\left(1+\chi_M\right)\right]$
C	$\left(\frac{\Delta f}{2}, \chi_M\right)$	$\left(\frac{1}{2}-\nu\right)\left[\chi_M f_s + \frac{\Delta f}{2}\left(1+\chi_M\right)\right]$
D	$\left(\frac{\Delta f}{2}, -\chi_M\right)$	$\left(\frac{1}{2}-\nu\right)\left[-\chi_M f_s + \frac{\Delta f}{2}\left(1-\chi_M\right)\right]$

Table 2. Values assumed by $g_2(\varepsilon, \chi)$ in the vertices of its domain $\mathcal{D}$.

2.1 Replica of the negative spectrum in (0, f_s/2)

This is the case when $\lambda = -1$ and $\nu = \lceil f_c/f_s \rceil > 0$, that is the nearest greater integer of f_c/f_s. According to (6), the actual value of f^* is

$$f^{*\prime} = -f_c + \nu f'_s = -f_c + \nu\,(f_s + \varepsilon)\,(1+\chi) \tag{16}$$

and (4), evaluated for the actual values of f_s and f^*, yields the same expression as in (9).

As already stated, the function g_1 assumes its maximum in one of the vertices of $\mathcal{D}$. A comparison of the values enlisted in Table 1 permits to affirm that the maximum is assumed in A, and the left side of (8) is maximized by

$$\frac{B + B_g}{2} - \nu\left[-\chi_M f_s - \frac{\Delta f}{2}\left(1-\chi_M\right)\right]. \tag{17}$$

Similarly, it is easy to show through pairwise comparisons that the function g_2 assumes its minimum in the point C, and the right side of (8) is maximized by

$$\frac{\left(f_s + \dfrac{\Delta f}{2}\right)\left(1+\chi_M\right) - \left(B + B_g\right)}{2} - \nu\left[\chi_M f_s + \frac{\Delta f}{2}\left(1+\chi_M\right)\right]. \tag{18}$$

According to (17) and (18), in the most restrictive case, the condition (9) can be rewritten as

$$\begin{cases} f^* < \dfrac{\left(f_s + \dfrac{\Delta f}{2}\right)(1+\chi_M) - \left(B + B_g\right)}{2} - \nu\left[\chi_M f_s + \dfrac{\Delta f(1+\chi_M)}{2}\right] \\ f^* > \dfrac{B + B_g}{2} + \nu\left[\chi_M f_s + \dfrac{\Delta f}{2}(1-\chi_M)\right] \end{cases}. \tag{19}$$

In conclusion, time-base resolution and time-base instability are responsible for a shifting of the replica included in $[0, f_s/2]$ from its expected central frequency f^*, and can consequently introduce unexpected aliasing, depending on the values of Δf and χ_M.

3. Optimal selection of the sample rate

The sample rate can be chosen within an infinite set of values, its choice having direct consequences on spectral location of replicas. The idea underlying the method proposed in (Angrisani & Vadursi, 2008) is to let the user choose where to place the replica characterized by the lowest central frequency and, consequently, automatically determine the lowest f_s that satisfies the choice, thus guaranteeing an optimal use of DAS resources. In particular, the main advantages consist in the optimization of DAS vertical resolution and memory resources, given the observation interval. On the basis of the results presented in Section 2, a method for the automatic selection of the DAS sample rate is hereinafter proposed. Two different implementations of the method are, in particular, given. The first proves appropriate when the sample clock is characterized by a constant resolution, as it happens when the DAS accepts an external sample clock. The second is addressed to variable sample clock resolution, which characterizes the cases when no external sample clock is either allowed or available and the DAS can vary its sample rate according to a specific rule.

3.1 Data acquisition systems with constant sample clock resolution

As it is evident from relation 1 and Fig. 1, replicas are not equally spaced on the frequency axis, and one and only one replica comes out to be centered in $(0, f_s/2)$. The first implementation allows the choice of the normalized frequency f^*/f_s. Specifically, the user can choose f^* in terms of a fraction of f_s:

$$f^* = f_s / p \quad , \qquad p > 2. \tag{20}$$

Moreover, the user can input a value for the minimum guard band between adjacent replicas. By substituting (20) into systems (15) and (19), it is possible to derive the conditions on f_s that must be respected in order to avoid aliasing. Such conditions are expressed as

$$\begin{cases} f_s > \dfrac{p}{1 - p|\nu|\chi_M}\left[\dfrac{B + B_g}{2} + |\nu|\dfrac{\Delta f}{2}(1+\chi_M)\right] \\ f^* > p\dfrac{B + B_g + \Delta f\left(|\nu| + \dfrac{1}{2}\right)(1-\chi_M)}{-2 + p(1-\chi_M) - 2p|\nu|\chi_M} \end{cases} \tag{21}$$

when $\lambda = 1$ (positive replica), and as

$$\begin{cases} f_s > \dfrac{p}{1-p|\nu|\chi_M}\left[\dfrac{B+B_g}{2}+|\nu|\dfrac{\Delta f}{2}\left(1-\chi_M\right)\right] \\ f^* > p\dfrac{B+B_g+\Delta f\left(|\nu|-\dfrac{1}{2}\right)\left(1+\chi_M\right)}{-2+p\left(1+\chi_M\right)-2p|\nu|\chi_M} \end{cases} \tag{22}$$

when λ = -1 (negative replica).
Once the user has entered the desired value of p, the algorithm provides the lowest f_s that verifies (20) and (21) (or (20) and (22), if $\lambda = -1$), given the bandwidth and the central frequency of the input signal, and the desired guard band between two adjacent replicas, B_g.
Let us impose $f^* = f_s / p$ in (1), and solve the equation with regard to f_s; the equation can be solved when either $\lambda = 1$ and $\nu \leq 0$, or $\lambda = -1$ and $\nu \geq 1$.
In such cases the solution is

$$f_s = \frac{\lambda\, p}{1-\nu\, p}\, f_c\,. \tag{23}$$

The set of possible values for $(1-\nu p)\backslash \lambda p$, arranged in increasing order, is

$$\left\{\frac{p-1}{p}, \frac{p+1}{p}, \frac{2p-1}{p}, \frac{2p+1}{p}, \ \ldots, \frac{n\,p-1}{p}, \frac{n\,p+1}{p}, \ldots\right\}. \tag{24}$$

The algorithm iteratively explores the set of solutions in (24), starting from the highest value for f_s, and halts when the current f_s does not respect either of the alias-free conditions (21) or (22) anymore. The last value of f_s which is compliant with the alias-free conditions is the lowest sample rate that provides the desired positioning of replicas and guarantees the minimum required guard band.

3.2 Data acquisition systems with variable sample clock resolution

When the resolution of the sample clock is variable, besides the inputs described in the previous case, the user is also required to give the set of possible sample rates allowed by the DAS. Since DAS's generally vary their sample rate according to the common 1:2:5 rule, i.e.

$$f_s \in \left\{\ldots, 10\ MHz, 20\ MHz, 50\ MHz, 100\ MHz, \ldots\right\} \tag{25}$$

a different approach is followed to find out the optimal value of f_s. In such a case, the set of possible values for f_s is, in fact, limited.
Due to the coarse-grained distribution of allowed values for f_s, the value of ε in (6) can be significantly too large, and induce intolerably large deviations from the expected value of f^*. Therefore, the adoption of the iterative algorithm described above would be meaningless, whereas an exhaustive approach should be preferred. Specifically, for each allowed value of f_s greater than twice the bandwidth of the signal, the corresponding value of f^* is calculated and the alias-free condition is checked.
In particular, only the effects of sample clock instability are taken into account, since the allowed values of f_s are given in input by the user; ε is therefore equal to 0. Then, the user

can select the preferred sample rate, on the basis of the corresponding values of f^* and of the frequency resolution (equal to f_s/N, N being the number of acquired samples).

4. Examples

The analytical results described in Section 2 show that taking into account finite time-base resolution and clock accuracy produces a modification of the values of the two thresholds given by (4). The new thresholds are given in (15) and (19).
Before giving details of the performance assessment of the proposed method, some application examples are proposed in order to evaluate how the optimal sample rate is affected by the new thresholds, how different the effects of finite time-base resolution and clock accuracy on the modification of the optimal sample rate are, and how aliasing is introduced when finite time-base resolution and clock accuracy are not properly considered.

4.1 First example

The case described hereinafter gives quantitative evidence of the modification introduced in the thresholds and, consequently, in the optimal sample rate, when finite time-base resolution and clock accuracy are included among input parameters. Let us consider a bandpass signal characterized by a bandwidth B = 3.84 MHz and a carrier frequency f_c = 500 MHz, and let us suppose that the values of B_g and p chosen by the user are equal to 0 and 3, respectively. Ignoring the effects of ε and χ would lead to an optimal sample rate, f_s, equal to 11.538461 MHz (Angrisani et al., 2004). On the contrary, when $\chi_M = 3.54 \cdot 10^{-4}$ and Δf = 10 Hz are taken into consideration, the optimal sample rate is 12.60504 MHz, which implies an increase of more than 9%. Let us go through the steps of the algorithm implementing the proposed method to evaluate how such modification is determined. Table 3 shows all the solutions of (23), that is all the sample rates meeting user's requirements, included between the aforementioned 11.538461 MHz and the suggested 12.60504 MHz, which is the optimal sample rate according to the new method. For each sample rate, Table 3 (*i*) states whether a positive (λ = 1) or negative (λ = -1) replica is located in the frequency range [0, $f_s/2$], (*ii*) gives the values of the thresholds $f_{1,old}$ and $f_{2,old}$, calculated according to (4) and utilized in (Angrisani et al., 2004), and (*iii*) provides the thresholds f_1 and f_2, calculated according to the new conditions (15) and (19). Looking at the table, the

f_s [MHz]	λ	f^* [MHz]	$f_{1,old}$ [MHz]	$f_{2,old}$ [MHz]	f_1 [MHz]	f_2 [MHz]
11.53846	1	3.84615	1.92000	3.84923	2.09585	3.67133
11.71875	-1	3.90625	1.92000	3.93938	2.09859	3.76285
11.81102	1	3.93700	1.92000	3.98551	2.09581	3.80760
12.00000	-1	4.00000	1.92000	4.08000	2.09862	3.90350
12.09677	1	4.03225	1.92000	4.12839	2.09577	3.95046
12.29508	-1	4.09836	1.92000	4.22754	2.09865	4.05106
12.39669	1	4.13223	1.92000	4.27835	2.09573	4.10041
12.60504	-1	4.20168	1.92000	4.38252	2.09868	4.20606

Table 3. Thresholds calculated according to the proposed method and that presented in (Angrisani et al., 2004). The signal under test is characterized by a bandwidth B = 3.84 MHz and a carrier frequency f_c = 500 MHz. Time-base resolution is 10 Hz and sample clock accuracy is $3.54 \cdot 10^{-4}$. The chosen value of p is equal to 10.

effects of finite time-base resolution and sample clock instability on the location of spectral replicas can be quantitatively evaluated; the critical threshold comes out to be the upper threshold f_2. In detail, if the signal is sampled at a rate equal to 11.538461 MHz, the replica is placed at a central frequency f^* equal to 3.84615 MHz, which meets the alias-free condition (4). As a consequence of the modification of the upper threshold from $f_{2,old}$ = 3.84923 MHz to f_2 = 3.67133 MHz, the value of 11.538461 MHz does not guarantee alias-free sampling anymore and has to be discarded. The same happens with successive solutions of (23): they all fail to fall within the new thresholds. The set of possible solutions of (23) has to be explored until 12.60504 MHz, which represents the minimum alias-free sample rate, is reached.

4.2 Second example

Let us consider a bandpass signal characterized by a bandwidth B = 140 kHz and a carrier frequency f_c = 595.121 MHz. Let us suppose that values of B_g and p chosen by the user are equal, respectively, to 0 and 10. The method in (Angrisani et al., 2004) would give an optimal sample rate, f_s, equal to 700.060 kHz. Table 4 gives the values of the optimal sample rate provided by the proposed method for different values of Δf ({1, 10, 100} Hz) and χ_M (between 10^{-8} and $3.54 \cdot 10^{-4}$). As expected, they are all greater than $f_{s,old}$ = 700.060 kHz. What is notable, they range from 704.369 kHz (when Δf = 1 Hz and $\chi_M = 10^{-8}$), which is within 1% from $f_{s,old}$, to 2.9158 MHz (when Δf = 100 Hz and $\chi_M = 3.54 \cdot 10^{-4}$), which represents an increase of more than 300%! Fig.2 permits to evaluate the different roles played by finite time-base resolution and clock accuracy in modifying the optimal sample rate with respect to that furnished by the method in (Angrisani et al., 2004). It shows the optimal sample rate versus clock accuracy, for different values of Δf. For lower values of χ_M, the most significant increase of f_s with respect to $f_{s,old}$ is mainly due to the resolution Δf and the curves are practically horizontal. As accuracy worsens (χ_M increases), the vertical difference among the three curves reduces, and becomes practically negligible for $\chi_M = 3.54 \cdot 10^{-4}$.
So, neither resolution nor accuracy can be said to prevail in determining the optimal sample rate.

Δf / χ_M	*100 Hz*	*10 Hz*	*1 Hz*
10^{-8}	998.3	740.29	704.369
10^{-6}	1003.4	745.85	710.253
$5.47 \cdot 10^{-6}$	1024.1	770.78	736.445
10^{-5}	1045.7	797.64	763.857
10^{-4}	1494.9	1319.26	1299.107
$3.54 \cdot 10^{-4}$	2915.8	2819.14	2819.143

Table 4. Optimal sample rate, expressed in kilohertz, for a bandpass signal characterized by a bandwidth B = 140 kHz and a carrier frequency f_c = 595.121 MHz, as a function of different values of time-base resolution and clock accuracy. The value of p has been chosen equal to 10.

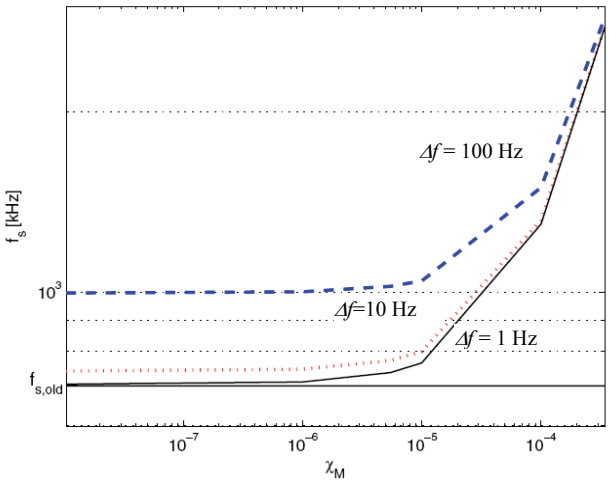

Fig. 2. Optimal sample rate versus clock accuracy, for different values of Δf . The bandpass signal under test has a bandwidth B = 140 kHz and a carrier frequency f_c = 595.121 MHz. The value chosen for p is 10.

4.3 Third example

This example refers to an experimental test conducted by means of the measurement station described in Section 5. Let us suppose that an external source, with a resolution Δf equal to 100 Hz, is utilized as DAS sample clock. The signal under test is a QAM (Quadrature Amplitude Modulation) signal, with bandwidth equal to 140 kHz and carrier frequency equal to 595.121 Hz. The value of p is chosen equal to 10. If the lowest alias-free sample rate that allows to place the lowest frequency replica at the normalized frequency $1/p$ was obtained through the application of an algorithm that does not take into account the finite resolution of the external source, a value of f_s equal to 700.060 kHz would be found, and the expected central frequency of the sampled signal would be 70.000 kHz. Rounding it to the nearest multiple of Δf would result in an actual sample rate of 700.1 kHz. As an effect of the rounding, the actual central frequency of the sampled signal would be 36.0 kHz, which means introducing unexpected, yet not negligible, aliasing. Fig. 3 shows the evolution versus time of the I baseband component measured from the sampled signal, referred to as I_{dem}, and the corresponding original one, assumed as reference, and referred as I. Similarly, Fig. 4 shows the evolution versus time of the Q baseband component measured from the sampled signal, and referred to as Q_{dem}, and the corresponding original one, assumed as reference, and simply as Q. The difference between the measured and reference signals, which is evident from the figures, is responsible for high values of the indexes ΔI (equal to 51%) and ΔQ (equal to 52%), defined in Section 5. On the contrary, an algorithm based on the analysis conducted in Section 2, which takes into account both finite time-base resolution and clock accuracy ($\chi_M = 3.54 \cdot 10^{-4}$, in this example), would produce a sample rate f_s = 2.9158 MHz, with a central frequency f^* = 297.8 kHz. No aliasing would occur, as Fig. 5 and Fig. 6 show, as the measured and the reference components are very close to each other. Values of ΔI and ΔQ lower than 5% are experienced.

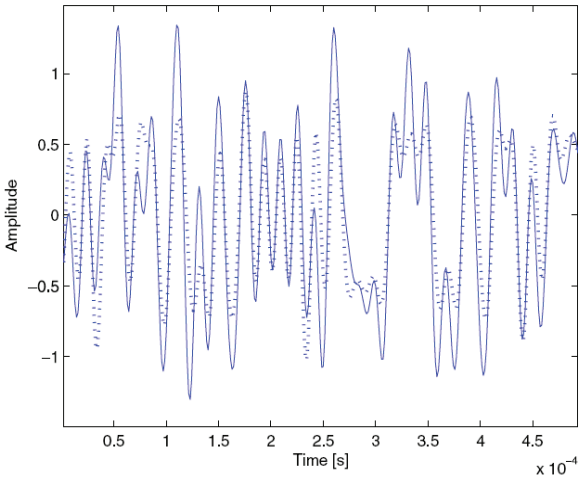

Fig. 3. Evolution versus time of measured I_{dem} (continuous line) and reference I (dotted line) with aliasing.

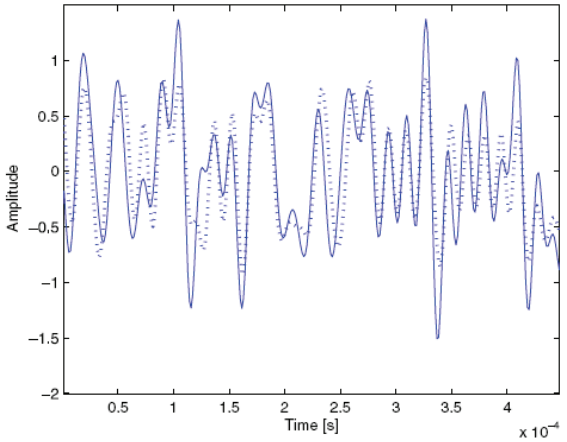

Fig. 4. Evolution versus time of measured Q_{dem} (continuous line) and reference Q (dotted line) with aliasing.

5. Performance assessment

A wide experimental activity has been carried out on laboratory signals to assess the performance of the two implementations of the method.

5.1 Measurement station

Fig. 7 shows the measurement station. The station consists of (*i*) a processing and control unit, namely a personal computer, (*ii*) a digital RF signal generator (250 kHz-3 GHz output

frequency range) with arbitrary waveform generation (AWG) capability (14 bit vertical resolution, 1MSample memory depth, 40 MHz maximum generation frequency), (*iii*) a DAS (8 bit, 1 GHz bandwidth, 8 GS/s maximum sample rate, 8 MS memory depth) and (iv) a synthesized signal generator (0.26-1030 MHz output frequency range), acting as external clock source; they are all interconnected by means of a IEEE-488 standard interface bus.

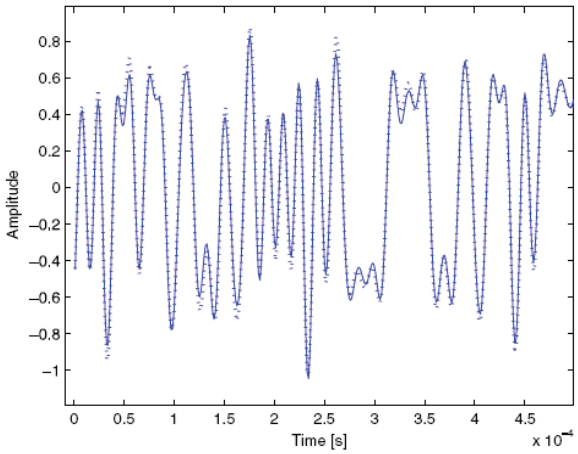

Fig. 5. Evolution versus time of measured I_{dem} (continuous line) and reference I (dotted line) without aliasing.

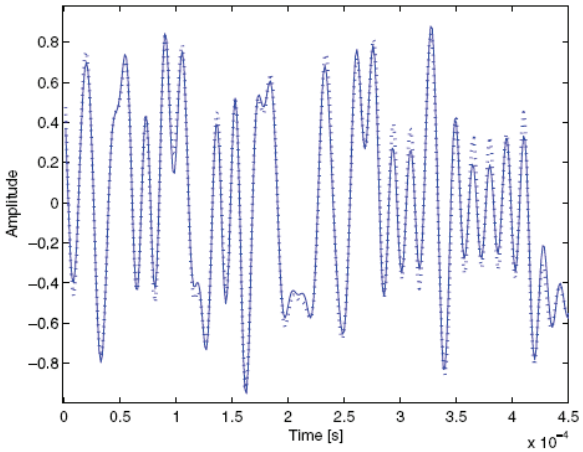

Fig. 6. Evolution versus time of measured Q_{dem} (continuous line) and reference Q (dotted line) without aliasing.

5.2 Test signals

A variety of digitally modulated signals have been taken into consideration, including M-PSK (M-ary Phase Shift Keying) and M-QAM (M-ary QAM) signals. Test signals have been

characterized by carrier frequency and bandwidth included, respectively, in the range 100 MHz-700 MHz and 100 kHz-5 MHz.

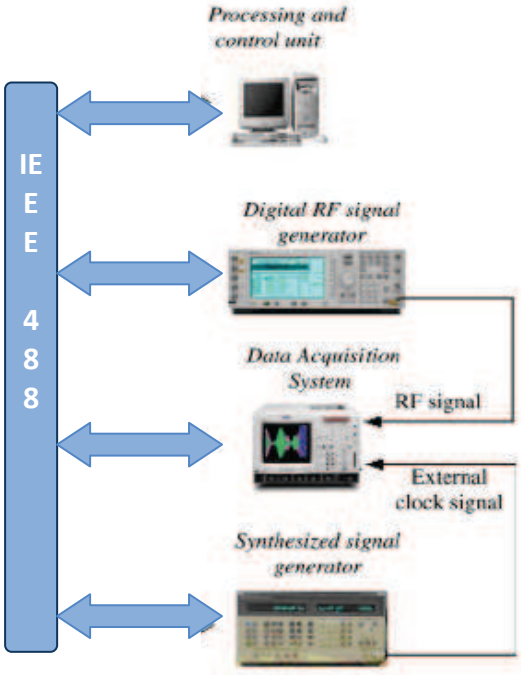

Fig. 7. Measurement station.

5.3 Measurement procedure

Experimental tests have been carried out according to the following procedure: 1) the digital RF signal generator produces a bandpass RF signal, characterized by known bandwidth and carrier frequency; 2) given the specified central frequency f^* and guard band B_g, the proposed method provides the optimal sample rate f_s; 3) in the case of external sample clock, the synthesized signal generator is commanded to output a sinusoidal signal characterized by a frequency value equal to f_s, otherwise the value of f_s is imposed as DAS sample rate; 4) the DAS digitizes the RF signal at a sample rate equal to f_s; 5) the processing and control unit retrieves the acquired samples from the DAS, through the IEEE-488 interface bus.

A two-domain approach has been used. The digitized signal has, in fact, been analyzed in the frequency and modulation domains to verify the concurrence of its actual central frequency with its expected value. With regard to frequency-domain, the difference between the actual and nominal central frequency, Δf^*, has been evaluated. In detail, the acquired samples have suitably been processed to estimate the power spectrum of the analyzed signal (Angrisani et al., 2003). Taking advantage of spectrum symmetry, the actual carrier

frequency has been measured as the threshold frequency that splits up the signal power in halves (Agilent Technologies, 2002). Concerning the modulation-domain, the digitized signal has gone through a straightforward I/Q demodulator, and tuned on the expected value of f^*, in order to gain the baseband components I_{dem} and Q_{dem}. I_{dem} and Q_{dem} have then been compared to the baseband components I and Q acquired from the auxiliary analog outputs of the digital RF generator and assumed as reference, in order to calculate the following indexes

$$\Delta I = \frac{1}{N}\sum_{i=1}^{N}\left|\frac{I_{dem}(i)-I(i)}{I(i)}\right|\times 100\% \tag{26}$$

$$\Delta Q = \frac{1}{N}\sum_{i=1}^{N}\left|\frac{Q_{dem}(i)-Q(i)}{Q(i)}\right|\times 100\% \,. \tag{27}$$

Moreover, EVM (Error Vector Magnitude), which is a key indicator for modulation quality assessment, has been evaluated. EVM bears traces of possible causes of signal impairments (Angrisani et al., 2005); its value, in particular, gets worse upon the increasing of the deviation of the central frequency increases from its expected value.

5.4 Results

With regard to frequency-domain analysis, Table 5 enlists the results obtained in the tests conducted on a QAM signal characterized by a bandwidth B = 3.84 MHz and a carrier frequency f_c = 500 MHz. Results are expressed in terms of percentage difference Δf^* between actual and expected central frequency of the replica, for different values of p, B_g, and Δf. Values of Δf^* lower than 1% prove the good performance of the method. Similar outcomes have been experienced with the other test signals taken into consideration.

Concerning modulation-domain analysis, the values of ΔI, ΔQ, and EVM, in percentage relative terms, have been, on average, equal to 3.5%. Considering that the demodulator utilized in the experiments is not optimized, the achieved results are extremely encouraging and prove the capability of the method in correctly placing the spectral replica at the desired frequency.

6. Conclusions

The chapter has presented a comprehensive method for automatically selecting the sample rate to be adopted by a DAS when dealing with bandpass signals. The method stems from a thorough analysis of the effects of sample clock instability and clock accuracy on the location on the frequency axis of spectral replicas of the sampled signal, and allows an automatic selection of the sample rate, in accordance to user's *desiderata*, given in terms of spectral location of the replicas and minimum guard band between replicas. Two alternative implementations have been presented, which refer to constant and variable time-base resolution of the DAS. The former can be applied when the DAS accepts an external clock source, whereas the latter is designed to work with the internal clock of the DAS that follows the common 1:2:5 rule.

		B_g [MHz]	f_s [MHz]	f^* [MHz]	Δf^* [%]
$p = 3$	$\Delta f = 10$ Hz	0	12.60504	4.20160	0.10
		1.16	16.30435	5.43485	0.12
		3.84	24.19355	8.06455	0.12
	$\Delta f = 100$ Hz	0	12.6050	4.2000	0.15
		1.16	16.3043	5.4333	0.20
		3.84	24.1935	8.0635	0.20
$p = 4$	$\Delta f = 10$ Hz	0	8.43882	2.10970	0.09
		1.16	10.81081	2.70274	0.19
		3.84	16.26016	4.06496	0.19
	$\Delta f = 100$ Hz	0	8.4388	2.1108	0.27
		1.16	10.8108	2.7032	0.33
		3.84	16.2602	4.0662	0.25
$p = 8$	$\Delta f = 10$ Hz	0	17.16738	2.14598	0.21
		1.16	21.62162	2.70274	0.18
		3.84	33.05785	4.13225	0.24
	$\Delta f = 100$ Hz	0	17.1674	2.1454	0.25
		1.16	21.6216	2.7032	0.25
		3.84	33.0579	4.1315	0.39

Table 5. Frequency-domain results related to a QAM signal with bandwidth B = 3.84 MHz and a carrier frequency f_c = 500 MHz. Sample clock accuracy is $3.54 \cdot 10^{-4}$.

Several experiments, carried out on digitally modulated signals, have assessed the performance of the proposed methods through a two-domain approach. Results have shown that the difference between actual and expected value of the central frequency of the sampled signal is very low ($\Delta f^* \leq 1.0\%$). Moreover, the baseband I and Q components have been reconstructed on the basis of the expected value of the central frequency. Thealues of ΔI, ΔQ, and EVM have, in fact, been on average lower than few percents.

7. References

Agilent Technologies (2002). Testing and troubleshooting digital RF communications transmitter designs. *Application Note 1313 Agilent Technologies Literature No.5968-3578E*.

Akos, D. Stockmaster, M. Tsui, J. & Caschera, J. (1999). Direct bandpass sampling of multiple distinct RF signals. *IEEE Trans. on Communications*. Vol.47, No. 7, (July 1999), pp.983-988.

Angrisani, L. D'Apuzzo, M. & D'Arco, M. (2003). A new method for power measurements in digital wireless communication systems. *IEEE Trans. Instrum. Meas.*. Vol.52. pp. 1097-1106.

Angrisani, L. D'Arco, M. Schiano Lo Moriello, R. & Vadursi, M. (2004). Optimal sampling strategies for bandpass measurement signals, *Proc. of the IMEKO TC-4 Interational Symposium on Measurements for Research and Industry Applications.* pp. 343-348, September 2004.

Angrisani, L. D'Arco, M. & Vadursi, M. (2005). Error vector-based measurement method for radiofrequency digital transmitter troubleshooting. *IEEE Trans. Instrum. Meas.*. Vol.54. pp. 1381-1387.

Angrisani, L. & Vadursi, M. (2008). On the optimal sampling of bandpass measurement signals through data acquisition systems. *IOP Meas. Sci. Technol.* Vol.19, (April 2008) 1-9.

Betta, G. Capriglione, D. Ferrigno, L & Miele, G. (2009). New algorithms for the optimal selection of the bandpass sampling rate in measurement instrumentation, *Proc. of XIX IMEKO World Congress*, pp. 485–490, September 2009.

Brown, J.L. (1980). First-order sampling of bandpass signals - A new approach. *IEEE Trans. on Information Theory*, Vol. 26, No. 5, (Sept. 1980), 613-615.

Corcora, J.J. (1999). Analog-to-Digital Converters, In: *Electronic Instrument Handbook,* C. F. Coombs (Ed.), Chapter 6, McGraw-Hill Professional, New York City, NY, USA..

Coulson, A.J. Vaughan, R.G. & Poletti, M.A. Frequency-Shifting Using Bandpass Sampling. *IEEE Trans. on Signal Processing*. Vol.42. No.6. pp.1556-1559.

De Paula, A. & Pieper, R.J. (1995). A more complete analysis for subnyquist bandpass sampling, *Proceedings of the 24th Southeastern Symp. on System Theory and the 3rd Annual Symp. on Communic., Signal Processing, Expert Systems, and ASIC VLSI Design,* March 1992.

Diez, R.J. Corteggiano, F. & Lima, R.A. (2005). Frequency mapping in uniform bandpass sampling, *Proceedings of the 24th Southeastern Symp. on System Theory and the 3rd Annual Symp. on Communic., Signal Processing, Expert Systems, and ASIC VLSI Design,* March 1992.

Gaskell, J. D. (1978). *Linear systems, Fourier transforms and optics.* Wiley. New York City, NY, USA.

Grace, O.D. & Pitt, S.D. (1968). Quadrature sampling of high frequency waveforms. *J. Acoustic Soc. Am.,* Vol. 44, pp. 1432-1436.

Jackson, M.C. & Matthewson, P. (1986). Digital processing of bandpass signals, *GEC J. Res.*, Vol. 4, No.1, 1986.

Kohlenberg, A. (1953). Exact interpolation of band-limited functions, *J. Appl. Phys.*, Vol. 24, 1432–1436.

Latiri, A. Joet, L. Desgreys, P. & Loumeau, P. (2006). A reconfigurable RF sampling receiver for multistandard applications. *Comptes Rendus Physique,* Vol. 7, No. 7, September 2006, pp. 785-793.

Ronggang, Q. Coakley, F.P. & Evans, B.G. (1996). Practical considerations for bandpass sampling. *Electronic Letters*. Vol.32. No. 20. Pp.1861-1862.

Shannon, C. (1949). Communication in the presence of noise, *Proc. IRE*, Vol. 37, 10–21.

Tseng, C.H. (2002). Bandpass sampling criteria for nonlinear systems. *IEEE Trans. on Signal Processing*, Vol. 50, No. 3, (March 2002).

Vaughan, R.G.; Scott, N.L.; White,D.R. (1991). The theory of bandpass sampling, *IEEE Trans. Signal Proc.,* Vol.39, No.9, (Sept. 1991) 1973-1984, ISSN

Waters, M. W.; Jarrett, B.R. (1982). Bandpass signal sampling and coherent detection, *IEEE Trans. Aerosp. Electron. Syst.*, Vol. AES-18, No. 4, (Nov. 1982).

Data Acquisition

Edited by Michele Vadursi

ISBN 978-953-307-193-0
Hard cover, 344 pages
Publisher Sciyo
Published online 28, September, 2010
Published in print edition September, 2010

The book is intended to be a collection of contributions providing a birdâ€™s eye view of some relevant multidisciplinary applications of data acquisition. While assuming that the reader is familiar with the basics of sampling theory and analog-to-digital conversion, the attention is focused on applied research and industrial applications of data acquisition. Even in the few cases when theoretical issues are investigated, the goal is making the theory comprehensible to a wide, application- oriented, audience.

How to reference

In order to correctly reference this scholarly work, feel free to copy and paste the following:

Leopoldo Angrisani and Michele Vadursi (2010). Bandpass Sampling for Data Acquisition Systems, Data Acquisition, Michele Vadursi (Ed.), ISBN: 978-953-307-193-0, InTech, Available from: http://www.intechopen.com/books/data-acquisition/bandpass-sampling-for-data-acquisition-systems

INTECH
open science | open minds

InTech Europe
University Campus STeP Ri
Slavka Krautzeka 83/A
51000 Rijeka, Croatia
Phone: +385 (51) 770 447
Fax: +385 (51) 686 166
www.intechopen.com

InTech China
Unit 405, Office Block, Hotel Equatorial Shanghai
No.65, Yan An Road (West), Shanghai, 200040, China
中国上海市延安西路65号上海国际贵都大饭店办公楼405单元
Phone: +86-21-62489820
Fax: +86-21-62489821